



Network Creation During Agglomeration Processes of Polydisperse and Monodisperse Systems of Droplets

Johannes Josef Schneider^{1,2} , Alessia Faggian³ , Aitor Patiño Diaz³ ,
Jin Li² , Silvia Holler³ , Federica Casiraghi³ , Lorena Cebolla Sanahuja³,
Hans-Georg Matuttis⁴, Martin Michael Hanczyc^{3,5} ,
David Anthony Barrow² , Mathias Sebastian Weyland¹ ,
Dandolo Flumini¹ , Peter Eggenberger Hotz¹, Pantelitsa Dimitriou² ,
William David Jamieson⁶ , Oliver Castell⁶ , Patrik Eschle¹ ,
and Rudolf Marcel Fuchslin^{1,7} 

¹ Institute of Applied Mathematics and Physics, School of Engineering,
Zurich University of Applied Sciences, Technikumstr. 9, 8401 Winterthur, Switzerland

johannesjosefschneider@googlemail.com,

{scnj,weyl,flum,eggg,escl,furu}@zhaw.ch

² School of Engineering, Cardiff University, Queen's Buildings, 14-17 The Parade,
Cardiff CF24 3AA, Wales, UK

{LiJ40,Barrow,dimitrioup}@cardiff.ac.uk

³ Laboratory for Artificial Biology, Department of Cellular,
Computational and Integrative Biology (CIBIO), University of Trento,
38123 Trento, Italy

{alessia.faggian,aitor.patino,silvia.holler,federica.casiraghi,
lorena.cebolla,martin.hanczyc}@unitn.it

⁴ Department of Mechanical Engineering and Intelligent Systems,
The University of Electrocommunications, Chofu Chofugaoka 1-5-1,
Tokyo 182-8585, Japan

hg@mce.uec.ac.jp

⁵ Chemical and Biological Engineering, University of New Mexico, MSC01 1120,
Albuquerque, NM 87131-0001, USA

⁶ Welsh School of Pharmacy and Pharmaceutical Science, Cardiff University,
Redwood Building, King Edward VII Avenue, Cardiff CF10 3NB, Wales, UK

{jamiesonw,Castell10}@cardiff.ac.uk

⁷ European Centre for Living Technology, S.Marco 2940, 30124 Venice, Italy
<https://www.zhaw.ch/en/about-us/person/scnj/>

Abstract. We simulate the movement and agglomeration of oil droplets
in water under constraints, using a simplified stochastic-hydrodynamic

This work has been partially financially supported by the European Horizon 2020
project *ACDC – Artificial Cells with Distributed Cores to Decipher Protein Function*
under project number 824060.

The original version of this chapter was previously published without open access.
A correction to this chapter is available at

https://doi.org/10.1007/978-3-031-31183-3_25

© The Author(s) 2023, corrected publication 2023

C. De Stefano et al. (Eds.): WIVACE 2022, CCIS 1780, pp. 94–106, 2023.

https://doi.org/10.1007/978-3-031-31183-3_8

model. We analyze both local and global properties of the networks formed by the agglomerations of droplets for various system sizes. We focus on the differences of these properties for monodisperse and polydisperse systems of droplets. For the mean degree, we obtain different values for critical exponents.

Keywords: Network analysis · monodisperse · polydisperse · droplets · cluster · agglomeration

1 Introduction

Within the scope of the European Horizon 2020 project *ACDC – Artificial Cells with Distributed Cores to Decipher Protein Function*, we intend to develop a probabilistic compiler [2, 20] to aid the three-dimensional agglomeration of particles filled with various chemicals in a specific way in order to e.g. create macromolecules via a gradual chemical reaction scheme [10, 11]. Hereby we aim at the creation of some specific macromolecules, but in contrast to the work of [7], we govern the successive reaction process by a specific design of the three-dimensional structure of the agglomeration. Furthermore, we are interested in the question of which molecules could be produced to which extent within randomly created agglomerations in comparison to the production within the primordial soup in order to have a closer look at the origin of life [9].

In such an agglomeration, neighboring droplets can form connections, either by simply touching each other or by getting glued to each other by matching pairs of single-stranded DNA, which are attached to hulls enclosing their surfaces. Chemicals contained within the droplets can move to neighboring droplets either directly, as hydrophobic compounds can be exchanged between adjacent oil droplets at the contact face, or, if the oil droplets are contained in a hull comprised of amphiphilic molecules like phospholipids, through pores within bilayers. Thus, a complex network is created, with the droplets being the nodes of this graph and the existing connections being the edges between the corresponding droplets.

In this paper, we present computational results for basic simulations of simplified agglomeration processes of oil droplets in water to mimic experiments. In the experiments performed by our co-authors at Cardiff University, a microfluidic approach is used to generate droplets: A stream of fluid within another fluid is split up in a series of spherical droplets of (almost) equal size after passing through a t-junction if the ratio of the pressures between the two fluid streams is chosen in an appropriate range [6]. In contrast, the manual emulsion method [3] called Rakka, which is used by our co-authors in experiments at the University of Trento, mechanically sends excitations in a large oil drop lying at the bottom of a container filled with water and containing amphiphilic molecules, thus splitting it in a polydisperse system of droplets with a wide range of radii. The droplets sink to the bottom of the cylinder where they agglomerate, while forming connections. Thus, this scenario of droplets randomly placed in a cylinder defines the starting point for the simulations.

Within the scope of this paper, we focus on the question of how polydispersity influences the agglomeration process of the particles and some specific properties of the networks created. In order to deal only with this question and to exclude effects from other experimental properties, we simulate the droplets as hard spheres and ignore details of the surface structure of the particles, attractive forces as well as adhesion effects. As the extension of the bilayers is very small and as due to their small radii [1], the droplets keep their spherical shape during the experiments, hence, this simplified approach is justified. This paper is organized as follows: In Sect. 2, we describe our simulation technique in detail, before presenting our computational results of a network analysis of the agglomerations both for polydisperse and for monodisperse systems of various system sizes in Sect. 3. Section 4 provides a summary of the results and an outlook to future work.

2 Simulation Details

At the beginning of the simulations, we randomly place N spherical particles in a cylindrical container with radius 1 mm and height 4 mm in a way that they do not overlap with each other and that they do not overlap with the walls of the cylinder, as shown in the left part of Fig. 1. For the polydisperse system, we randomly choose the particle radii r_i uniformly from the interval $[10-50] \mu\text{m}$, whereas we set all radii $r_i \equiv 30 \mu\text{m}$ for the monodisperse system.



Fig. 1. Initial (left) and final (right) configuration generated in a simulation of the agglomeration process of a multidisperse system of 2,000 spherical particles in a cylinder.

After this initialization, we perform the main simulation which is comprised of 10^7 time steps of a duration of $\delta t = 10^{-5}$ s. In each time step, the particles are subjected to various forces:

- They sink in water due to gravity \mathbf{F}_G reduced by the buoyant force \mathbf{F}_b :

$$\mathbf{F}_G(i) - \mathbf{F}_b(i) = \frac{4\pi}{3} r_i^3 (\rho_{\text{oil}} - \rho_{\text{water}}) g \quad (1)$$

For the oil density, we use the value $\varrho_{\text{oil}} = 1.23 \text{ kg/l}$, just as in the experiments of our co-authors in Trento.

- Secondly, the spatial components $v_{x,y,z}(i)$ of the velocity vectors $\mathbf{v}(i)$ are subjected to random velocity changes: They are randomly altered by up to $\pm 5\%$ of their absolute values in order to take at least in this small random way into account that the containers are moved by the experimentalists in the laboratory in Trento.
- The particles are also subjected to the Stokes friction force \mathbf{F}_S :

$$\mathbf{F}_S(i) = -6\pi\eta r_i \mathbf{v}(i) \quad (2)$$

The viscosity of water at 25°C is $\eta = 0.891 \text{ mPas}$.

- As in classic hydrodynamics, the concept of added mass [19] is used. When applying Newton's second law, we have to consider an effective mass of the particle, i.e., $\mathbf{F}(i) = m_{\text{eff}}(i)\mathbf{a}(i)$. This effective mass is composed of the mass $m(i)$ of particle i and of the added mass $m_{\text{added}}(i)$. This added mass is caused by the inertia of the surrounding fluid, which needs to be deflected or attracted if the particle itself is accelerated or decelerated in the water, and can be determined to being half of the mass of the water displaced by oil particle i . Thus, we use for the deceleration caused by the Stokes friction the equation

$$\mathbf{a}_S(i) = \frac{\mathbf{F}_S(i)}{m(i) + m_{\text{added}}(i)}. \quad (3)$$

When working with such a set of second order differential equations governing the laws of motion for the particles, the question arises as to which integrator to use. Due to the stochastic nature of random velocity changes, only an Euler scheme with very small time intervals is suitable for the determination of new velocities and positions [4]. In the case of collisions between pairs of particles or between particles and walls, a mostly elastic collision dynamics is imposed. Overlaps occurring at the end of each time step are resolved as in [8, 12].

When simulating a polydisperse and a monodisperse system of droplets, generating movies from these simulations, and watching them, one sees at first sight a striking difference between polydisperse and monodisperse systems: While the droplets in a monodisperse system sink to the bottom of the cylinder with almost equal speed, in the case of the polydisperse system the largest droplets rush down fastest, whereas the smallest droplets sink comparatively very slowly towards the bottom of the cylinder. Also the agglomeration processes at the bottom of the cylinder look different as the final agglomerations themselves. Thus, we evaluate these agglomerations and their time evolutions with some standard measures from network analysis in order to quantify these differences.

For this purpose, we performed 100 simulation runs each both for the polydisperse and for the monodisperse system for the system sizes $N = 10, 20, 30, 40, 50, 60, 70, 80, 90, 100, 110, 120, 130, 140, 150, 160, 170, 180, 190, 200, 250, 300, 350, 400, 450, 500, 550, 600, 650, 700, 750, 800, 850, 900, 950, 1000, 1100, 1200, 1300, 1400, 1500, 1600, 1700, 1800, 1900, 2000, 2500, 3000, 3500, 4000, 4500,$ and 5000 . From each simulation run, we store each 1000th configuration,

such that we have a set of 10^4 configurations per simulation run, with a time interval of 0.01 s between successive configurations. The results presented for the network analysis in the next section are averaged over the measurements taken from the 100 simulations. Thus, for each curve in Figs. 2, 4, 6, and 8 in total 10^6 configurations had to be evaluated.

3 Network Analysis

For network analysis, first of all a network related to the problem to be considered has to be defined. As we are interested mainly in structures resulting from neighborhood relationships, we have a look at the adjacency matrix η with

$$\eta(i, j) = \begin{cases} 1 & \text{if droplets } i \text{ and } j \text{ are neighbors of each other} \\ 0 & \text{otherwise.} \end{cases} \quad (4)$$

We consider a pair (i, j) of droplets as neighboring each other, meaning (almost) touching each other, if the condition

$$\sqrt{(x_i - x_j)^2 + (y_i - y_j)^2 + (z_i - z_j)^2} \leq r_i + r_j + 0.1 \mu\text{m} \quad (5)$$

is fulfilled, i.e., if the distance between their midpoints is smaller or equal to the sum of their radii plus some small offset. Please note that one usually sets $\eta(i, i) \equiv 0$ for all nodes i . The matrix η contains all the information about the network.

When analyzing a network, one mostly takes either an atomistic view, looking at the various nodes and determining their network related properties, or a global view, determining clusters of nodes and dealing with questions like whether the network is percolating [18]. We present basic results both for the atomistic and for the global view.

3.1 Degrees of the Particles

As an example for local network analysis, we consider the degrees of the particles. A degree $k(i)$ of a node i is defined as the number of nodes it is attached to via edges in the network. It can be easily calculated by

$$k(i) = \sum_{j=1}^N \eta(i, j). \quad (6)$$

We are interested in the average $\langle k \rangle$ of all degrees, its time evolution, and its final value for various system sizes, both for the polydisperse and for the monodisperse systems.

Figure 2 shows the increase of $\langle k \rangle$ over time t for various system sizes N . The increases are steeper for the monodisperse system and approach their final values less smoothly than in the case of the polydisperse system. Furthermore,

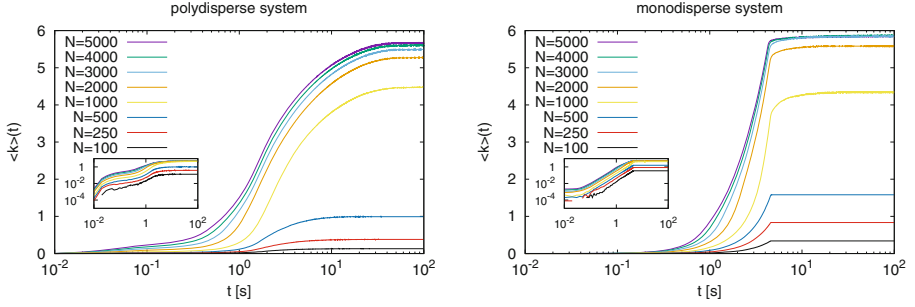


Fig. 2. Time evolution of the average value $\langle k \rangle$ of the degrees for various system sizes: On the left, results for the polydisperse system are presented, on the right, results for the monodisperse system are shown. In the insets, the curves are redrawn in a double-logarithmic way to put more emphasis on short time scales.

the insets reveal that $\langle k \rangle$ increases in a double-sigmoidal way for the polydisperse system, while this is not the case for the monodisperse system, for which only one sigmoidal increase can be observed. The final values for $\langle k \rangle$ are larger for small and large system sizes for the monodisperse system, such that we now have a closer look at the final values also for other system sizes.

Figure 3 depicts the final values for various system sizes, both for the polydisperse system and for the monodisperse systems. In both cases, we find that there are regimes of system sizes in which we can fit the data points to various specific fit functions well known from the studies of phase transitions and order parameters in statistical physics [17]. Besides the linear or quadratic increase for small N , we find an interesting critical behavior. When investigating the data points for the polydisperse system in Fig. 3, we get the overall behavior [15]

$$\langle k_f \rangle = \begin{cases} c_1 N & \text{for } N \leq 40 \\ c_1 N + c_2 N^2 & \text{for } N \leq 80 \\ c_3 \frac{N^\alpha}{(N_{\text{crit},1} - N)^\gamma} & \text{for } 40 \leq N \leq 900 \\ c_4 \tanh\left(c_5 (N - N_{\text{crit},2})^\beta\right) & \text{for } 850 \leq N \end{cases} \quad (7)$$

with the prefactors c_1, \dots, c_5 , the critical exponents α, β , and γ , and the critical numbers $N_{\text{crit},1}$ and $N_{\text{crit},2}$ of particles. Various fits of the functions in Eq. 7 with similar fitting qualities result in $\alpha = 1 \dots 1.1$, $\gamma = 0.4 \dots 0.5$, $\beta = 0.1 \dots 0.18$, $N_{\text{crit},1} = 940 \dots 1000$, and $N_{\text{crit},2} = 780 \dots 845$. Please note that the prefactor $c_4 = 6 \dots 7$ provides an estimate for $\langle k_f \rangle$ in the limit $N \rightarrow \infty$. While the values for prefactors and critical numbers of particles will change if altering the simulation parameters, the theory of critical phenomena decrees that the critical exponents α, β , and γ and the form of the functions stay identical [17].

For the monodisperse system, we find striking similarities, but also differences to the polydisperse system. Here we get a linear increase of $\langle k_f \rangle$ for $N \leq 160$, a critical increase for $200 \leq N \leq 900$ according to the same law as for the

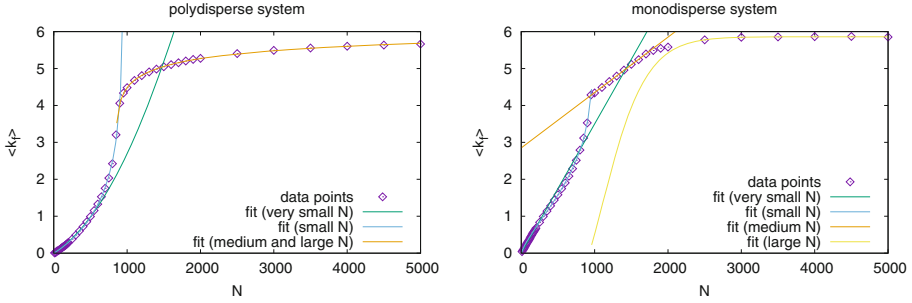


Fig. 3. Final values $\langle k_f \rangle$ for the averages of the degrees for various system sizes N : Both for the polydisperse (left) and for the monodisperse system (right), we find ranges of N for which we can fit the data points to specific fit functions: for the polydisperse system, the data points are fitted to $1.2 \times 10^{-3}N + 1.5 \times 10^{-6}N^2$ for $N \leq 80$, to $2.222848282 \times 10^{-2} \times N^{1.064929} / (982.95 - N)^{0.4597383}$ for $40 \leq N \leq 900$, and to $6.4592928303905470 \tanh(0.41066892597996169 \times (N - 843.037477864008)^{0.14512724870611132})$ for $850 \leq N \leq 5000$. For the monodisperse system, we display the fit functions $3.5 \times 10^{-3}N$ for $N \leq 160$, $4.9962568900578735 \times 10^{-2} \times N^{0.78025269698399657} / (1008.0838515966243 - N)^{0.22394426252398117}$ for $200 \leq N \leq 900$, $2.85 + 1.5 \times 10^{-3} \times N$ for $950 \leq N \leq 1700$, and $5.8606051850230925 \tanh(7.4870316562044323 \times 10^{-4} \times (N - 923.86956752140270)^{1.1002364522169625})$ for $1900 \leq N \leq 5000$. The more exactly given fit parameters were determined with an altered conjugate gradients method [16].

polydisperse system, but then in contrast to the polydisperse system a linear increase for $950 \leq N \leq 1700$, and finally we tried to fit a tangens hyperbolicus also to the data points in the regime of large $N \geq 1900$. However, this last fit to a tangens hyperbolicus is of a worse quality, the data points are not sufficient to prove that we have this same behavior here. The small value for c_4 here suggests that the assumption of a tangens hyperbolicus might be wrong in the case of a monodisperse system. For the largest values $N \geq 3000$, the measured averages of $\langle k_f \rangle$ might simply fluctuate in the range $[5.84 - 5.87]$. These results do not prove but seem to hint that in the limit $N \rightarrow \infty$, the final average value for $\langle k_f \rangle$ is significantly larger for the polydisperse system than for the monodisperse system.

In the next step, we have a look at the time evolutions of the maximum degree $k_{\max} = \max\{k(i)\}$ for various system sizes, which are shown in Fig. 4. For the polydisperse system, we find a sigmoidal increase. In the case of the monodisperse system, the increase is steeper, but is then stopped rather abruptly when reaching the final values $k_{\max,f}$. These final values are shown in Fig. 5. We find that $k_{\max,f}$ is slightly larger for the monodisperse system for small system sizes, but then the curves cross in the range $500 \leq N \leq 700$. From then on, $k_{\max,f}$ is larger for the polydisperse system. For the monodisperse system, $k_{\max,f}$

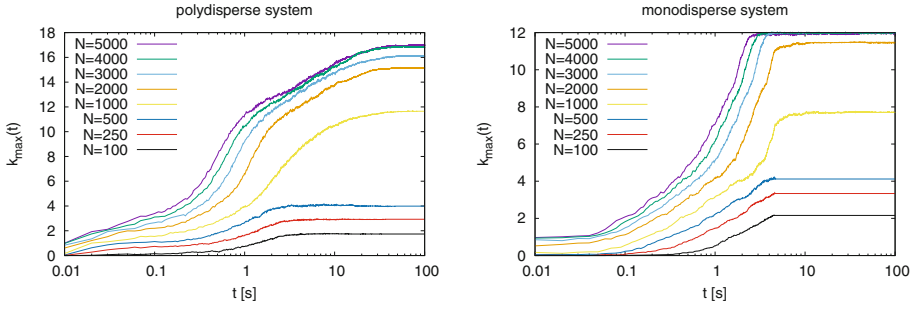


Fig. 4. Time evolution of the maximum k_{\max} of the degrees for various system sizes, both for the polydisperse system (left) and for the monodisperse systems (right).

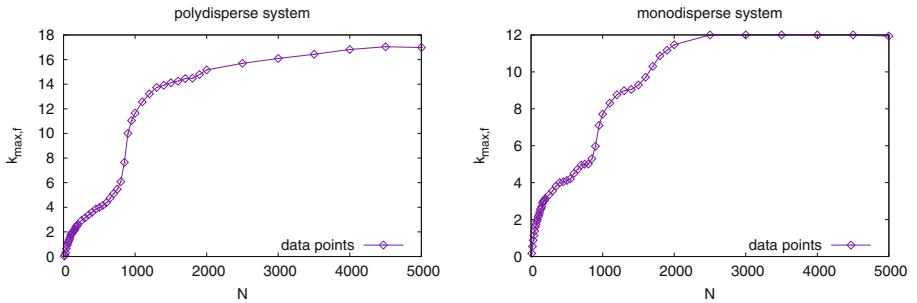


Fig. 5. Final values $k_{\max,f}$ of the maximum of the degrees for various system sizes, both for the polydisperse system (left) and for the monodisperse systems (right).

is bounded by the kissing number of 12 in three dimensions [5, 13]. Also the polydisperse system contains such a bound, depending on the ratio between the radii of the largest and of the smallest particles, but this bound is considerably larger in our case, in which this ratio is 1:5 [13], such that it does not play a role here as $k_{\max,f}$ is much smaller for the system sizes we consider here.

3.2 Clusters of Particles

As an example for global network analysis, we present results for the decrease of the number of clusters and the increase of the maximum cluster size. A cluster is defined as a subset C of nodes in the network for which the condition holds that for each arbitrarily chosen pair (i, j) of nodes with $i, j \in C$, a path from i to j exists on which one walks only over edges starting at a node in C and ending at a node in C , and for which no node is left out which fulfills this condition.

We are interested in the number N_c of clusters and its time evolution for various system sizes both for the polydisperse and for the monodisperse systems. As the droplets are placed in the cylinder at the beginning of the simulation without touching each other, we generally get $N_c = N$ at the beginning of the

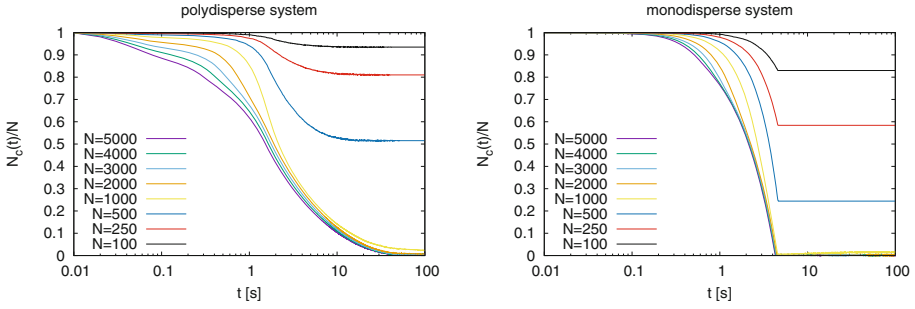


Fig. 6. Time evolution of the number N_c of clusters, renormalized by the number N of particles for various system sizes, both for the polydisperse system (left) and for the monodisperse systems (right).

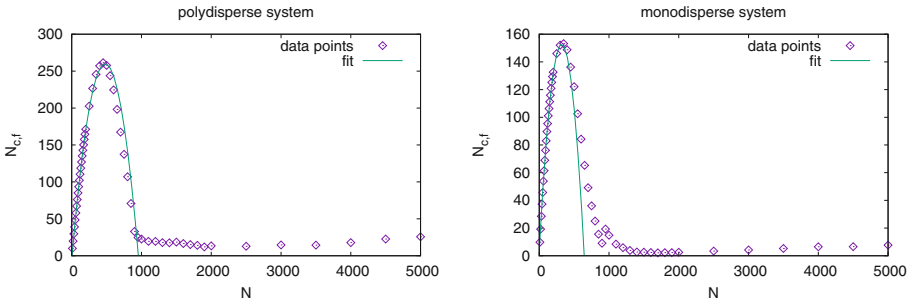


Fig. 7. Final values $N_{c,f}$ of the number of clusters for various system sizes, both for the polydisperse system (left) and for the monodisperse systems (right): The fit function for the polydisperse system is given by $260 - 0.00115 \times (N - 480)^2$, for the monodisperse system by $153 - 0.00145 \times (N - 321)^2$.

simulation, as each node forms a cluster of its own at the beginning. (Please note that we also count these “one-node clusters”.) With an increasing number of edges, clusters unite and N_c decreases. In order to better compare the results for various system sizes, we plot the number N_c renormalized by the system size N in Fig. 6. We get a sigmoidal decrease for the polydisperse system, but again we find an abrupt end of the decrease for the monodisperse system when the final value $N_{c,f}$ is reached, which is plotted in Fig. 7. Both for the polydisperse and for the monodisperse system, we find that the final number of clusters can be fitted almost quadratically for small system sizes N . For large system sizes, the number of clusters does not decrease to 1, but a small number of clusters remains.

Thus, the question arises whether the system is split in various clusters of almost equal size or in various clusters with strongly differing sizes or whether the system is dominated by one large cluster. Therefore, we have a look at the size C_{\max} of the largest cluster, which is the number of nodes contained in this

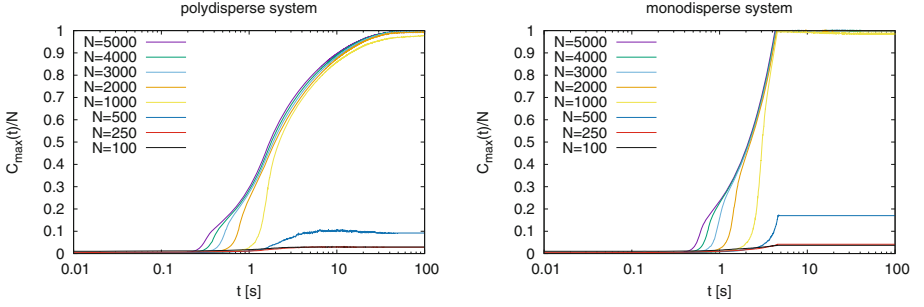


Fig. 8. Time evolution of the size C_{\max} of the largest cluster, renormalized by the number N of particles for various system sizes, both for the polydisperse system (left) and for the monodisperse system (right).

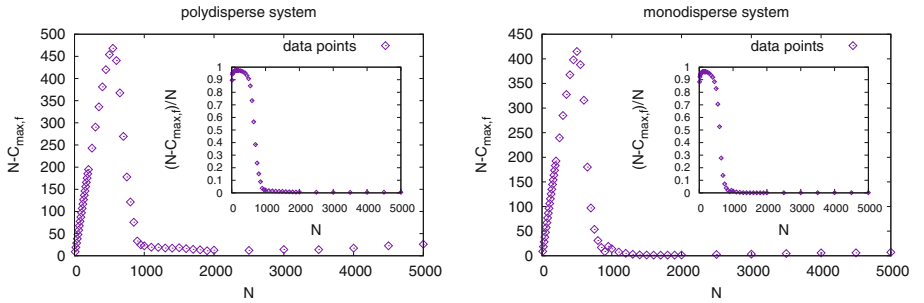


Fig. 9. Deviation of the final values of the size $C_{\max,f}$ of the largest cluster from the system size, for various system sizes, both for the polydisperse system (left) and for the monodisperse system (right). In the insets, the data points are replotted to display the relative deviation of C_{\max} from the system size.

cluster. In order to again better compare the results for the time evolution of this observable, we renormalize it with the system size and plot C_{\max}/N in Fig. 8. This ratio increases sigmoidally over time, reaching a value of (almost) 1 for large system sizes. Again, the increase stops abruptly for monodisperse systems when the final value $C_{\max,f}$ is reached. When plotting $C_{\max,f}$ versus the system size N , one only sees a linear increase of $C_{\max,f}$ for medium and large N [15]. Thus, we here have a look at the absolute deviations $N - C_{\max,f}$ of these final values from the corresponding system sizes and at the relative deviations $(N - C_{\max,f})/N$, which are plotted in Fig. 9. Both for the polydisperse and for the monodisperse system, we see an almost linear increase of the absolute deviation at small system sizes, which is reflected by a virtually constant value of the relative deviation, which is slightly smaller than 1. Then the absolute and the relative deviation decrease to relatively small values till $N = 1000$. For larger system sizes, only 12–28 droplets are on average not part of the largest cluster for the polydisperse system. In the case of the monodisperse system, this number is even smaller,

here only 1–2 droplets are not part of the largest cluster for most large system sizes. Thus, we generally find that the systems always end up with a dominating cluster containing almost all particles.

4 Conclusion and Outlook

In this paper, we presented results of simulations for the agglomeration of polydisperse and monodisperse systems of droplets. As we are interested in the effects of polydispersity on the agglomeration process and on the resulting droplet networks, we study a very simplified system, in which the droplets are represented as hard spheres (There are no other attractive or repulsive forces implemented.), subjected to gravity reduced by buoyancy, as well as Stokes friction, added mass effect, random velocity changes, and almost-elastic impacts. Connections between these particles are virtually formed if they (almost) touch or overlap. The particles gradually agglomerate at the bottom of the cylindrical container. The analysis of this agglomeration process from a local and a global point of view shows that the results for the time evolution and the final outcome strongly depend both on the number of particles and on the question whether we have to deal with a polydisperse or a monodisperse system. In particular, we find two transition regimes: at small numbers N of particles, we find an over time gradually increasing number of droplets lying finally at the bottom of the cylinder where they either stay isolated or gradually form pairs and then some slightly larger groups with other particles reaching the bottom as well. When increasing N even further, a network of droplets is created at a bottom layer of the cylinder. During this regime, we find first an increase of the number of clusters and then a decrease again due to the formation of one gradually more dominating cluster containing most droplets.

We intend to continue our investigations by measuring clustering coefficients, fractal dimensions, the locations of droplets with differing radii, and the importance some droplets might have for the overall network. Furthermore, we will perform simulations also with other simulation parameters, like another size of the cylinder and with other polydisperse radius distributions in order to better understand the values for the critical exponents and for the critical numbers and their dependencies. We also plan to extend our investigations first to binary systems, in which two particle types A and B are present and connections can only be forged between pairs of $A-B$ but not $A-A$ or $B-B$ [14] and then to ternary systems, in which there are three particle types A , B , and C with connections between adjacent pairs of $A-B$ particles but in which the additional C -particles are unable to form any connections. Hereby we want to study the breakdown of the size of the largest cluster with increasing density of C -particles. Furthermore, we want to add gluing forces between particles to find out how they change the results.

References

1. Aprin, L., Heymes, F., Laureta, P., Slangen, P., Le Floch, S.: Experimental characterization of the influence of dispersant addition on rising oil droplets in water column. *Chem. Eng. Trans.* **43**, 2287–2292 (2015)
2. Flumini, D., Weyland, M.S., Schneider, J.J., Fellermann, H., Füchslin, R.M.: Towards programmable chemistries. In: Cicirelli, F., Guerrieri, A., Pizzuti, C., Socievole, A., Spezzano, G., Vinci, A. (eds.) WIVACE 2019. CCIS, vol. 1200, pp. 145–157. Springer, Cham (2020). https://doi.org/10.1007/978-3-030-45016-8_15
3. Hadorn, M., Boenzli, E., Eggenberger Hotz, P., Hanczyc, M.M.: Hierarchical unilamellar vesicles of controlled compositional heterogeneity. *PLoS ONE* **7**, e50156 (2012)
4. Kloeden, P., Platen, E.: Numerical Solution of Stochastic Differential Equations. SMAP, Springer, Heidelberg (2013). <https://doi.org/10.1007/978-3-662-12616-5>
5. Kucherenko, S., Belotti, P., Liberti, L., Maculan, N.: New formulations for the kissing number problem. *Discret. Appl. Math.* **155**, 1837–1841 (2007)
6. Li, J., Barrow, D.A.: A new droplet-forming fluidic junction for the generation of highly compartmentalised capsules. *Lab Chip* **17**, 2873–2881 (2017)
7. Marshall, S.M., et al.: Identifying molecules as biosignatures with assembly theory and mass spectrometry. *Nat. Commun.* **12**, 3033 (2021)
8. Müller, A., Schneider, J.J., Schömer, E.: Packing a multidisperse system of hard disks in a circular environment. *Phys. Rev. E* **79**, 021102 (2009)
9. Oparin, A.: *The Origin of Life on the Earth*, 3rd edn. Academic Press, New York (1957)
10. Schneider, J.J., Weyland, M.S., Flumini, D., Füchslin, R.M.: Investigating three-dimensional arrangements of droplets. In: Cicirelli, F., Guerrieri, A., Pizzuti, C., Socievole, A., Spezzano, G., Vinci, A. (eds.) WIVACE 2019. CCIS, vol. 1200, pp. 171–184. Springer, Cham (2020). https://doi.org/10.1007/978-3-030-45016-8_17
11. Schneider, J.J., Weyland, M.S., Flumini, D., Matuttis, H.-G., Morgenstern, I., Füchslin, R.M.: Studying and simulating the three-dimensional arrangement of droplets. In: Cicirelli, F., Guerrieri, A., Pizzuti, C., Socievole, A., Spezzano, G., Vinci, A. (eds.) WIVACE 2019. CCIS, vol. 1200, pp. 158–170. Springer, Cham (2020). https://doi.org/10.1007/978-3-030-45016-8_16
12. Schneider, J.J., Müller, A., Schömer, E.: Ultrametricity property of energy landscapes of multidisperse packing problems. *Phys. Rev. E* **79**, 031122 (2009)
13. Schneider, J.J., et al.: Geometric restrictions to the agglomeration of spherical particles. In: Schneider, J.J., Weyland, M.S., Flumini, D., Füchslin, R.M. (eds.) WIVACE 2021. CCIS, vol. 1722, pp. 72–84. Springer, Cham (2022). https://doi.org/10.1007/978-3-031-23929-8_7
14. Schneider, J.J., et al.: Influence of the geometry on the agglomeration of a polydisperse binary system of spherical particles. In: *The 2021 Conference on Artificial Life, ALIFE 2021* (2021). <https://doi.org/10.1162/isal.a.00392>
15. Schneider, J.J., et al.: Paths in a network of polydisperse spherical droplets. In: *The 2022 Conference on Artificial Life, ALIFE 2022* (2022). <https://doi.org/10.1162/isal.a.00502>
16. Schneider, J.J., Kirkpatrick, S.: *Stochastic Optimization*. Springer, Heidelberg (2006)
17. Stanley, H.E.: *Introduction to Phase Transitions and Critical Phenomena*. Oxford University Press, New York (1972)

18. Stauffer, D., Aharony, A.: Introduction to Percolation Theory. Taylor & Francis (1992)
19. Stokes, G.G.: On the effect of the internal friction of fluids on the motion of pendulums. Trans. Cambridge Philos. Soc. **9**, 8–106 (1851)
20. Weyland, M.S., Flumini, D., Schneider, J.J., Füchslin, R.M.: A compiler framework to derive microfluidic platforms for manufacturing hierarchical, compartmentalized structures that maximize yield of chemical reactions. In: The 2020 Conference on Artificial Life, ALIFE 2020, pp. 602–604 (2020). <https://doi.org/10.1162/isa.l.a.00303>

Open Access This chapter is licensed under the terms of the Creative Commons Attribution 4.0 International License (<http://creativecommons.org/licenses/by/4.0/>), which permits use, sharing, adaptation, distribution and reproduction in any medium or format, as long as you give appropriate credit to the original author(s) and the source, provide a link to the Creative Commons license and indicate if changes were made.

The images or other third party material in this chapter are included in the chapter's Creative Commons license, unless indicated otherwise in a credit line to the material. If material is not included in the chapter's Creative Commons license and your intended use is not permitted by statutory regulation or exceeds the permitted use, you will need to obtain permission directly from the copyright holder.

